# Detection, Excision and Statistics of Interference at the Mauritius Radio Telescope

S. Sachdev[1,2] & N. Udaya Shankar[1,2, *]

[1]*Raman Research Institute, Sadashivanagar, Bangalore 560 080, India*
[2]*Department of Physics, University of Mauritius, Reduit, Mauritius.*

**Abstract.** A technique to detect man-made interference in the visibility data of the Mauritius Radio Telescope (MRT) has been developed. This technique is based on the understanding that the interference is generally 'spiky' in nature and has Fourier components beyond the maximum frequency which can arise from the radio sky and can therefore be identified. We take the sum of magnitudes of visibilities on all the baselines measured at a given time to improve detectability. This is then high-pass filtered to get a time series from which the contribution of the sky is removed. Interference is detected in the high-pass data using an iterative scheme. In each iteration, interference with amplitudes beyond a certain threshold is detected. These points are then removed from the original time series and the resulting data are high-pass filtered and the process repeated. We have also studied the statistics of the strength, numbers, time of occurrence and duration of the interference at the MRT. The statistics indicate that most often the interference excision can be carried out while post-integrating the visibilities by giving a zero weight to the interference points.

*Key words.* Metre-wave radio telescope—Fourier synthesis—interference excision.

## 1. Introduction

Mauritius Radio Telescope (MRT) is a new metre-wave radio telescope operating at 150 MHz. The primary objective of the telescope is to produce a sky survey in the declination range $-70°$ to $-10°$ with a point source sensitivity of about 200 mJy ($3\sigma$). This will be the southern sky equivalent of the Cambridge 6C survey. A detailed description of the telescope is to be found in Golap *et al*. (1998). Mauritius was chosen as the site for the new telescope due to its strategic geographic location (latitude = $-20.14°$), where the Galactic Centre is almost overhead. The island was also considered a paradise for low frequency astronomy due to its interference-free environment. Unfortunately it no more remains an interference-free site due to the industrial growth in the country. This has confirmed the general belief that a totally interference-free

---

*email*: uday@rri.res.in

site may be a thing of the past, especially at low frequencies. In Mauritius the band around 150 MHz is not a primary allocation for radio astronomy. The Government of Mauritius has allocated only a 1 MHz band from 150 MHz to 151 MHz and not the band from 150.05 to 153 MHz, generally allocated to radio astronomy (Handbook on Radio Astronomy 1995). Emission from a new communication facility operating at 149 MHz, spills into the protected band making it unusable for radio astronomy. There is also interference from unidentified satellite(s) in this band. We have therefore moved the frequency of operation from the initially planned 150 MHz to 151.5 MHz. A narrow band around 151.5 MHz is relatively free of interference. Since this is not a protected band in Mauritius, an application for protection of this frequency has been forwarded to the Government of Mauritius.

In the mean time we have carried out observations with the MRT for more than 20,000 hours and data analyses are in progress. The section 2 of this paper briefly describes the Mauritius Radio Telescope and the observations carried out for the survey. The next section describes problems related to local interference and basic principles used for detection of external interference. Section 4 gives the description of the algorithm developed with a few illustrations of interference detection. In section 5 we give the statistics of the interference observed. Section 6 describes the principles used for interference mitigation in the final images.

## 2. The Mauritius Radio Telescope

The Mauritius Radio Telescope (MRT) is a Fourier synthesis T-shaped array with an East-West (EW) arm of length 2048m having 1024 helical antennas. The South (S) arm consists of a rail line of length 880m and 16 movable trolleys each with four helical antennas. The 1024 helices in the EW arm are divided into 32 groups of 32 helices each. All the EW groups are not at the same height, a situation imposed by the uneven terrain. Each trolley in the S arm constitutes one S group.

The 48 group outputs are amplified, heterodyned to 30 MHz in the field and brought separately to the observatory building via coaxial cables. In the observatory, the 48 group outputs are further amplified and down converted to a second IF of 10.1 MHz. The 32 EW and 16 S group outputs are fed into a $32 \times 16$ complex, 2-bit 3-level digital correlator sampling at 12 MHz. The 512 complex visibilities are integrated and recorded at intervals of 1 second. At the end of 24 hours of observation the trolleys are moved to a different position and new visibilities are recorded. The S baselines are sampled with a spacing of 1m, which is half a wavelength at 150 MHz. A minimum of 60 days of observing are needed to obtain the visibilities up to the 880m spacing. The Fourier Transform of the phase corrected visibilities obtained after the complete observing schedule, produces a map of the area of the sky under observation with a synthesized beam of $4' \times 4.6' \sec(\delta + 20.14°)$. The expected root mean square (RMS) noise in the image made using an IF bandwidth of 1 MHz and an integration time of 8 seconds is $\approx$200 mJy($3\sigma$).

The full width at half maximum (FWHM) of the primary beam of a S $\times$ EW interferometer at MRT is $2° \times 60°$. Due to this broad primary beam and its low operating frequency, the MRT is very susceptible to terrestrial interference. Interference causes spurious features in an image. If these effects are greater in strength than the noise fluctuations, they lead to misinterpretation. Hence, it is important to remove this interference. Interferences discussed in this paper can be classified as local and external

depending upon the locations of their sources. Here interference from sources which are located in-house are classified as local, while external refers to interference from sources remote to the telescope.

## 3. Local interference

Local interference is due to oscillators used in the observatory, whose harmonics fall in the observing band or the IF band.

We found the oscillators in switch mode power supplies of Personal Computers to be the main source of Radio Frequency Interference (RFI) emanating from the observatory building. These and the other parts of the receiver system were shielded by putting them in grounded Faraday cages. The analog and digital parts were grounded separately. Since the telescope site is rocky, the natural grounding is not good. Three pits, each 3m deep, with copper grounding plates buried in a mixture of coal and salt were used to improve the grounding. Two of these were used to separately ground the digital and analog parts of the receiver system. The third pit was used as ground for the air-conditioners and the computer systems outside the receiver room. The observatory building was not built with shielding. We reduced the effect of interference from the observatory by covering it with grounded stainless steel mesh.

To reduce the effect of common-mode interference picked up by the first IF cables and by the second IF signal lines, phase switching of the LO was implemented. We were also faced with the noise generated by the LO generator at 30 MHz, the first IF frequency. This leaked to the IF port at the first mixer and produced high correlations in some of the baselines. To reduce this, we used a band elimination filter centered around 30 MHz in the path of the Local Oscillator (LO).

The first IF at 30 MHz, is heterodyned with an LO of 40 MHz. In this conversion, stray signals centered around 50 MHz, picked up by long cables carrying the first IF to the observatory building, gets into the observing band. This resulted in increased noise in the observing band. To reduce their effects, we introduced band-pass filters centered around 30 MHz just before the heterodyning.

After sorting out most of the problems related to "in-house" interference, we still had interference in our data from external sources. The next section discusses the interference from external sources.

### 3.1 *Interference detection*

Some of the well known sources of external interference are communication systems, ignition systems of vehicles moving close to the telescope, high voltage power lines, satellites and the active Sun. Many of these produce short-interval, 'spiky' interference which have frequency components at a much higher frequency than that of the response of the antenna to celestial sources. Interference from man-made sources is highly polarized. Interference from communication systems is also generally narrow-band. However, interference with a broader spectrum is produced by arcing sources.

The front end of the receiver system has been built with sufficient bandwidth so that the observing frequency can be shifted (within 145–155 MHz) to an interference-free zone by tuning the LO. Presently the telescope is operated at 151.5 MHz which allows maximum interference-free observations.

At the MRT, since we do not measure the polarization of the signal, we cannot use this property of interference in differentiating the interference from the sky signal. Furthermore since we use XF correlators, we cannot reject parts of the observing band in which the interference occurs and use the rest of the band.

The 'spiky' nature of the interference is used for its detection at MRT. Interference which is 'spiky' in nature generally has Fourier components beyond the maximum due to the sky signal. In interferometer arrays, the visibility data are generally sampled in time at rates much faster than the rates required for a given baseline. This can be made use of in identifying interference which is 'spiky' in nature. For example, at the MRT the baseline with the longest east-west component ($\sim 512\lambda$) has a maximum fringe rate of about 0.04 Hz. We have sampled the data every one second which allows us to identify frequencies up to 0.5 Hz. Therefore interference can be identified by its contribution to frequencies in the range 0.04 Hz to 0.5 Hz.

The maximum frequency to which the sky contributes at the output of a complex correlator is given by $\omega_e x$, where $\omega_e = dH/dt = \frac{2\pi}{(24 \times 60 \times 60)} = 7.27 \times 10^{-5}$ radians per sidereal second and $x$ is the east-west component of the baseline in wavelengths. Since $x$ depends on the baseline used, the ability to distinguish interference from the sky signal decreases with increasing east-west component of the baseline. To overcome this baseline dependence, instead of detecting interference in the *cosine* and the *sine* channels separately, interference is detected in the magnitude of the visibility i.e., in $\sqrt{\cos^2 + \sin^2}$. The magnitude of visibility has a rate of change which is independent of the baseline used. This rate depends on the primary beam of the interferometer which is the product of the voltage patterns of a group of antennas (EW and S groups) forming the interferometer. At MRT the primary beam of the interferometer used for imaging is $2° \times 60°$. Thus the expected maximum frequency at the MRT in the magnitude of the visibility is $\sim$0.003 Hz.

The best method to ensure detection of interference in the *sum of magnitudes* would be to look for interference in the resultant obtained by summing all possible combinations of baselines. For example, if the interference had affected only two interferometers, then this interference would best be detected if the detection was carried out on the summation of magnitudes of these two baselines only, instead of adding the contribution of all the baselines. This, however, is not practical in terms of analysis time. We find that generally, interference affects all baselines simultaneously. Therefore, to improve the detectability of interference we add the magnitudes of all the visibilities used. We refer to this combined data as the *sum of magnitudes*.

The last group of the East array (E16) is fed to the correlator in the place of the 16th trolley of the S array. This gives a set of baselines formed between E16 and the E-W array on all observing days. This set of baselines is useful for calibration but reduces the number of usable trolleys to only 15. Thus only 480 ($15 \times 32$) baselines are used for imaging. If the magnitudes of all the visibilities of these 480 baselines are added, we will be able to detect interference at the level of $5\sigma_m/\sqrt{480}$ with a $5\sigma$ detection, where $\sigma_m$ is the RMS noise on the $\sqrt{\cos^2 + \sin^2}$ of any baseline and $\sigma$ is the RMS noise on the *sum of magnitudes*. For statistical considerations, a detection level greater than five times the RMS of the noise is used. Assuming interference affects all baselines with equal strength, we are able to detect interference down to $5\frac{\sigma_m}{\sqrt{480}}$, i.e., $\frac{\sigma_m}{4.4}$ per baseline. On the other hand if only $n$ baselines are affected, then an interference of strength less than $\frac{5\sigma_m\sqrt{480}}{n}$ per baseline would go undetected.

At MRT images are made by adding 60 days of data. Further four images are post-integrated to get a final image. Assuming that there is interference on only one of the sixty days at a given sidereal time, the undetected interference will be of the order of the noise in this final image. This, in terms of flux density, is of the order of 100 mJy.

In principle, the process of combining visibilities of different baselines may also be extended to the data of different days to further detect interference which occurs at the same right ascension on some other day. Since this is very unlikely we decided to allow undetected interference of the order of $\frac{\sigma_m}{4.4}$ in the final images.

By detecting interference in the *sum of magnitudes* (incoherent detection), the sensitivity to detection is $\sqrt{2}$ times worse than detection carried out on phased visibilities (coherent detection). In using *sum of magnitudes*, there is the advantage of the simplicity of looking at one time series.

## 4. Implementation scheme

In the implementation of the detection of interference, the *sum of magnitudes* is low-pass filtered. This is done by applying a rectangular window function on the Fourier transform of the *sum of magnitudes* data. This retains only those frequencies corresponding to the sky contribution. The low pass filter allows a maximum frequency of $\omega_e x$, where $x$ is the maximum east-west spatial frequency. For an EW × NS interferometer, $x = 36\lambda$. The output of this filter, which contains frequencies up to $\omega_e x$, is Inverse Fourier Transformed (IFT). This is then subtracted from the visibility data resulting in the 'difference' data from which the sky contribution has been removed. This 'difference' data is basically a high pass data with frequencies greater than $\omega_e x$, i.e., greater than the sky response. This therefore may be considered to consist only of contributions from the receiver noise and from the interference. The interference is detected in this 'difference' data. The detected points are stored in a file and are used to reject these points in subsequent processing. The flow diagram shown in Fig. 1 summarizes the technique used.

We now look at different ways of detecting the interference to minimize the time required without losing the reliability of the detections.

We started with a brute-force method in which the maximum deviation is located in the 'difference' data. If this deviation is greater than $k\sigma$, it is noted as interference. Here $\sigma$ is the expected RMS deviation due to the receiver noise in the 'difference' data and $k$ determines the threshold level of detection. This noted point is then removed from the time series and the remaining data are passed through the high pass filter again. This process is repeated till no points beyond $k\sigma$ are detected in the 'difference' data.

This method although simple and effective is prohibitively slow as it requires a filtering operation (involving an FFT and an IFT) for every interference point.

To reduce the time required we used an algorithm in which the interference is treated as a set of delta functions. In the 'difference' data a delta function appears convolved with the high pass function. In this algorithm, the maximum greater than $k\sigma$ is detected as earlier. However, instead of removing the marked out point in the time series and doing the whole process all over again, the high-pass response of a delta function of strength equal to the detected interference is subtracted from the 'difference' data. A delta function whose height equals the
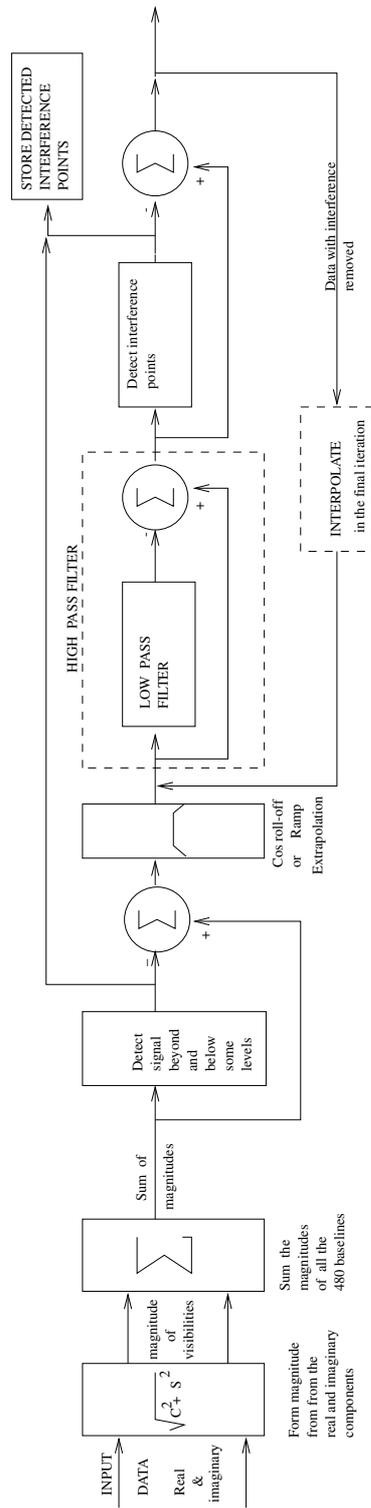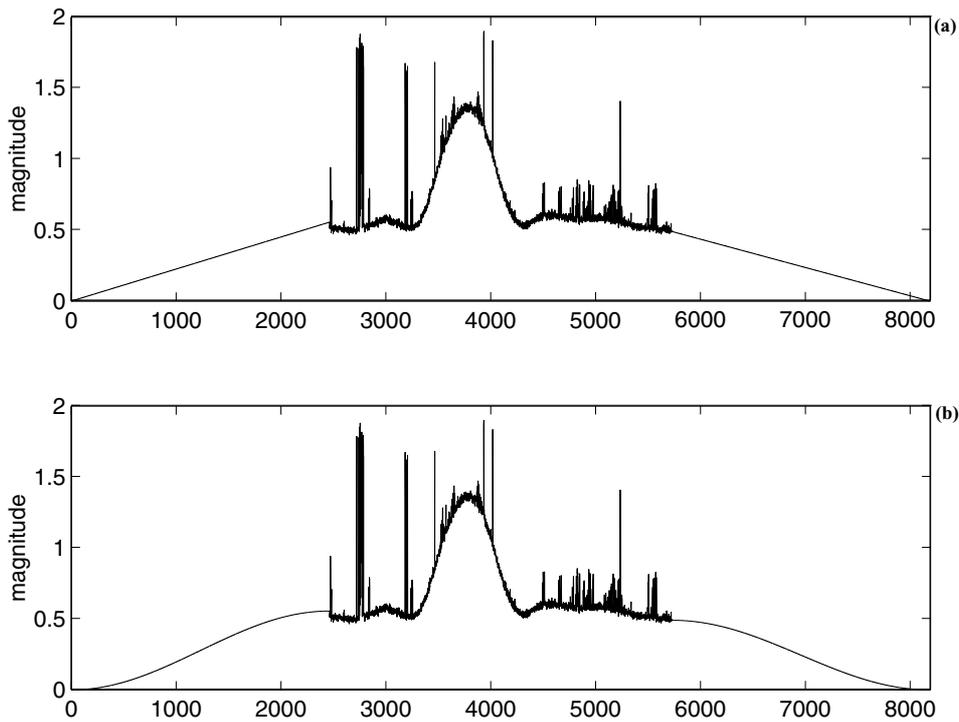
**Figure 1.** Block diagram illustrating the method adopted for interference detection.

**Figure 2.** *Extrapolation*: The data at the beginning and at the end of a file are extrapolated with **(a)** a ramp function **(b)** cosine roll-off function.

maximum that has been subtracted is placed in a separate file. The next highest point in the residual difference data is then located and the procedure is repeated until a pre-determined level is reached in the residual difference. This is essentially performing a 'deconvolution' using the CLEAN algorithm (Hogbom 1974) on the 'difference' data. All detected points are then removed from the visibility data.

Some erroneous detections occur if there are strong, closely spaced interference which results in a very distorted 'difference' data. To overcome such a problem the following alternative algorithms were tried out:

(a) Whenever an interference point is found, a scaled high pass response due to the interference (which is the response of the high pass filter to a delta function) is removed. This is similar to introduction of a 'loop gain' in standard CLEAN algorithms.

(b) The interference is detected in the 'difference' data above a certain threshold level which is set depending on the maximum interference level. In each iteration interference points of strength greater than 80% of the peak interference detected are removed. We found that this method gives better results than the method (a) and is therefore used in the final implementation of interference detection.

A few practical aspects in interference detection are listed below.

1. Most correlators give a finite, non-zero correlation even for uncorrelated inputs. Because of these offsets, the magnitudes of the visibilities have higher frequency
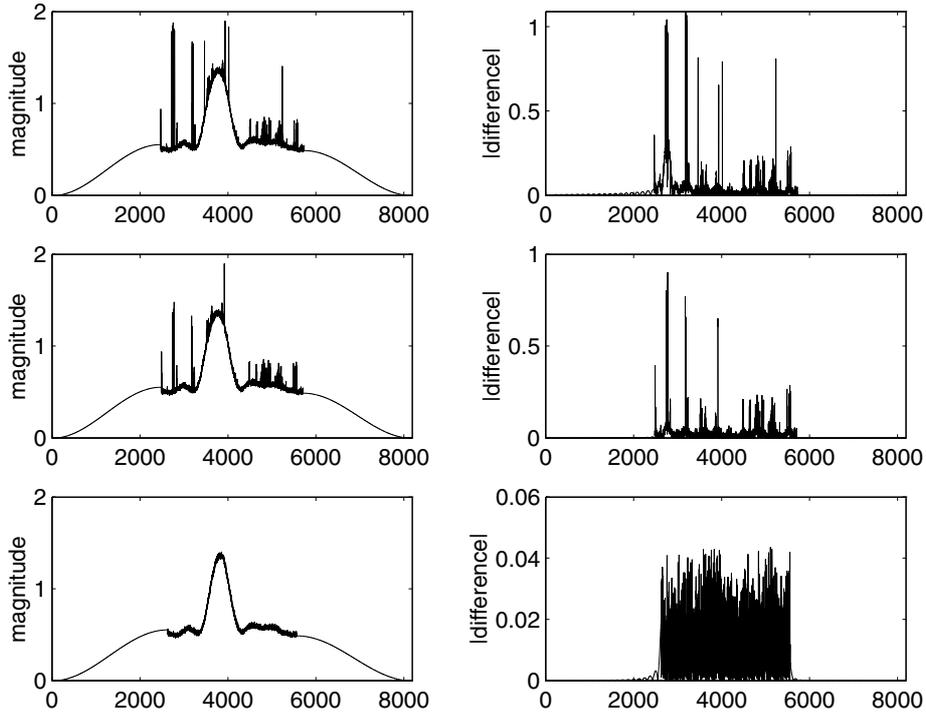
**Figure 3.** The different stages in interference detection. The left panels show the extrapolated *sum of magnitudes* and the right panels show the corresponding 'difference' data. The results of the 1st, 5th and the 15th, which is the last iteration, are shown.

components than the cut-off criterion used[1]. In the *sum of the magnitudes*, the contribution of these frequency components due to any given baseline is only $\frac{1}{480}$. Hence these are not detected as interference. But one would need to take this into account when applying the technique on a lesser number of baselines where the contribution of the fringing component produced by the offsets could be significant.

2. Using a DFT causes ripples whenever there is an offset between the beginning and the end of the patch being Fourier transformed [2]. Depending on the strength of the ripple, this may be detected as interference. To overcome this, the data at the beginning and at the end of the file are extrapolated with a smooth function before performing DFT. We find that using a cosine roll-off or a ramp function for extrapolation is generally sufficient. An example of the ramp extrapolation and cosine roll-off extrapolation is shown in Fig. 2. The cosine roll-off is better because it does not have a discontinuity at the edges. A larger extrapolation results in a smoother transform. The standard practice would be to use windowing which

---

[1] $\sqrt{(A + \cos(\omega t))^2 + (B + \sin(\omega t))^2} = \sqrt{A^2 + B^2 + 1 + 2A\cos(\omega t) + 2B\sin(\omega t)} = \sqrt{A^2 + B^2 + 1 + K\cos(\omega t - \phi)}$ . $A$ and $B$ are the offsets in the cos and the sin channels respectively. $\phi = \tan^{-1}\frac{B}{A}$ and $K = 2\sqrt{A^2 + B^2}$.

[2] In a DFT algorithm the patch being transformed is treated as being periodic.
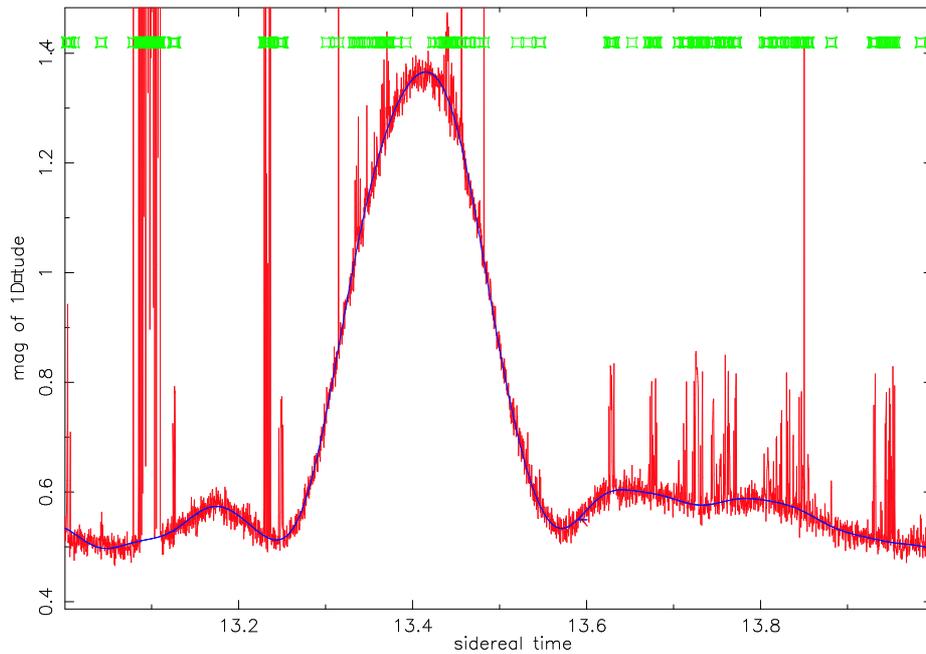
**Figure 4.** Interference detection on the *sum of magnitudes*: Detected interference points are marked out. Overlaid on the data is the fit to the data after removal and interpolation of the interference points from the *sum of magnitudes*.

would require data before and after the patch over which we are trying to detect interference. Using the 'smoothing' extrapolation we are able to process any size of data.

3. Response due to a strong source partially appearing at the beginning or at the end of a patch being processed will have a rate of change much higher than that expected from the sky and therefore would get removed as interference. This is prevented by increasing the length of the extrapolating function at the edge whenever a source of significant strength ($\geq 30\sigma$ in the *sum of magnitudes*) is encountered at the edge of a patch being processed.

4. An upper-cutoff and a lower-cutoff level are introduced based on *a priori* information of the highest and the lowest levels of the signals from the sky being processed. Any data point which is larger than, or less than, the limiting value is expunged from the data before any filtering is carried out. This reduces the time to process interference detection as the number of iterations are greatly reduced. The cut-off levels for any sidereal time take into account the changes in the Sun's right ascension.

5. We examined the difference between *sum of magnitudes* of two days (same trolley allocation) after removal of interference and interpolation to look for slowly varying interference not detected by our procedure.

6. As a final measure, the *sum of magnitude* plots after interference removal and interpolation are visually inspected and any suspicious looking data are manually identified.
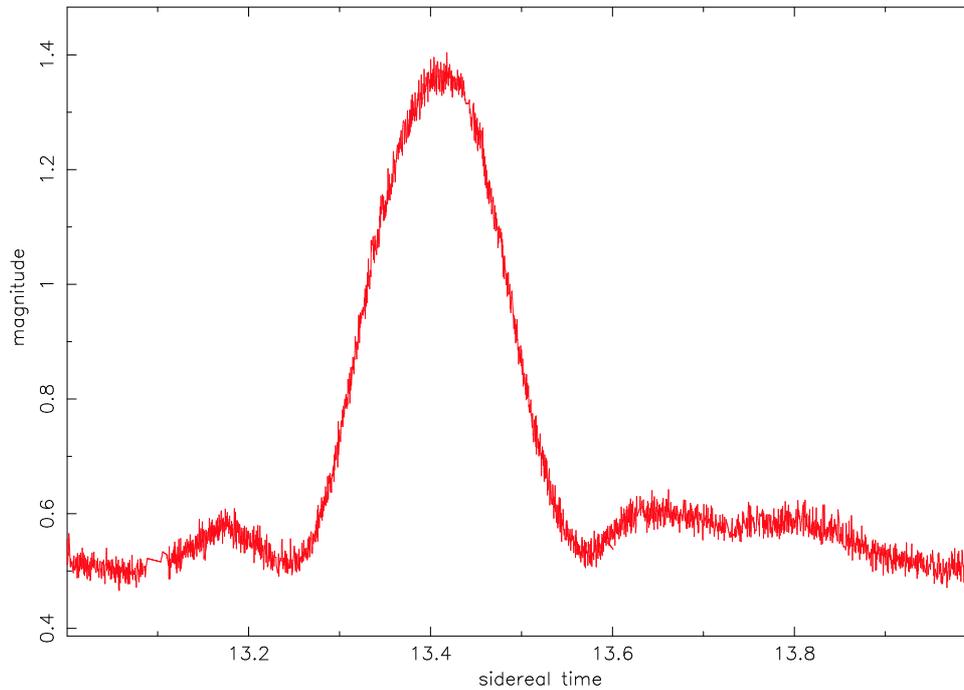
**Figure 5.**  *Sum of magnitudes* after removal of interference and interpolation.

At the MRT, programs have been developed to implement the above algorithm
(Sachdev 1999). The process of interference detection has been automated (except
steps 5 and 6) and is carried out at the end of each sidereal hour. An example of the
different stages in interference detection is shown in Fig. 3 with the column on the left
showing the *sum of magnitudes* and the column on the right showing the corresponding
'difference' data. Fig. 4 shows all the interference points which have been detected.
The *sum of magnitude* after removal of the interference points and interpolation is
shown in Fig. 5.

## 5.  Statistics of detected interference

We have data from observations over a year and have carried out interference detection
on this data. We now look at the statistics of the detected interference.

- A typical histogram of the number of interference points against their strengths
  is shown in Fig. 6. From the histogram we note that most of the interference
  points have strengths less than $100\sigma$ ($\approx 85\%$). We find $N\ \alpha\ K^{-0.8}$, where $N$ is
  the number of interference points with a strength K $\sigma$.
- Figure 7 is a histogram of interference points against strength of interference
  up to $500\sigma$. The number of interference points do not fall monotonically and
  occasionally there is a large number of interference points at around $70\sigma$ and
  $100\sigma$.
- Figure 8 shows the number of interference points against the number of consecu-
  tive seconds an interference lasts. We see that the largest number of interference
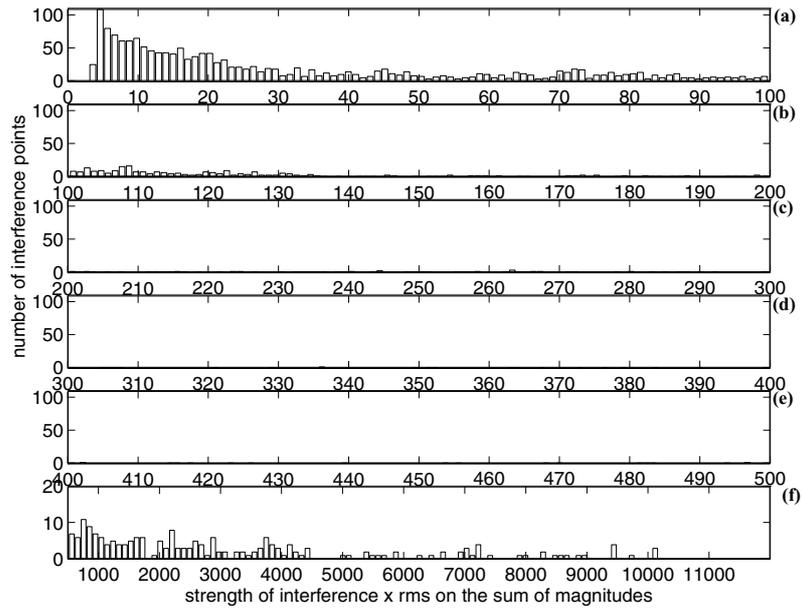
**Figure 6.** Histogram of number of interference points versus the strength of interference. All plots have 100 bins. **(a)** up to $100\sigma$ **(b)** from $100\sigma$ to $200\sigma$ **(c)** from $200\sigma$ to $300\sigma$ **(d)** from $300\sigma$ to $400\sigma$ **(e)** from $400\sigma$ to $500\sigma$ **(f)** from $500\sigma$ to max interference level
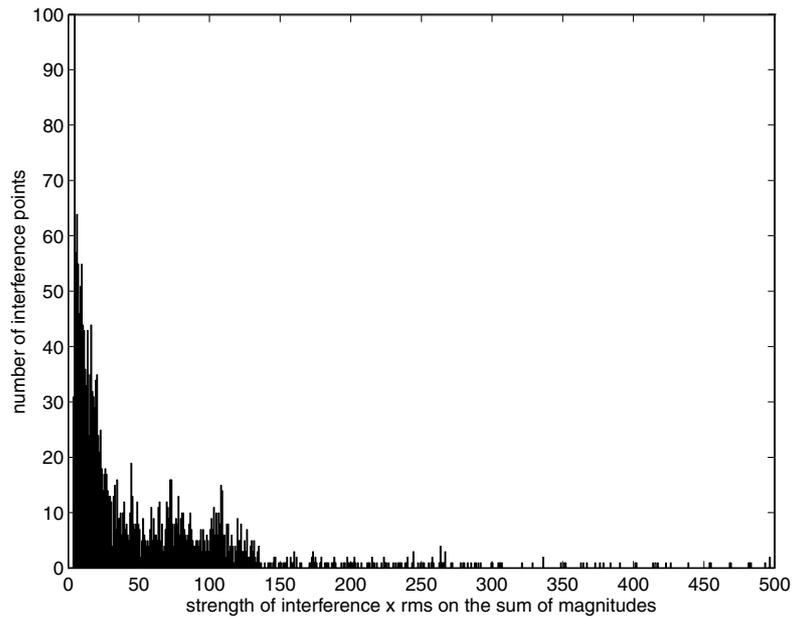


**Figure 7.** Histogram of number of interference points versus the strength of interference up to $500\sigma$.
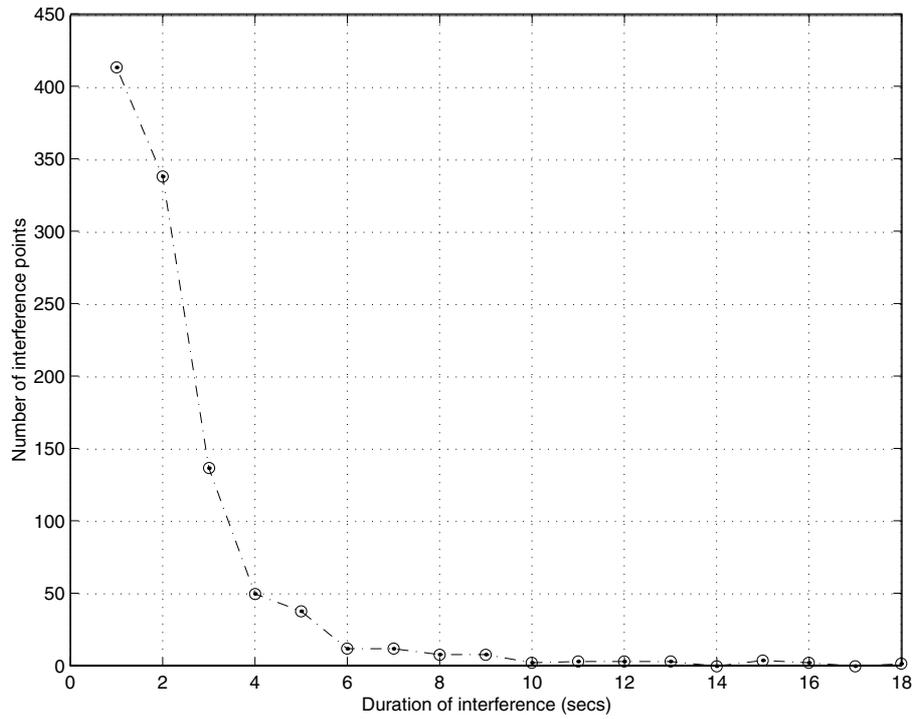
**Figure 8.** Statistics of the duration of interference.
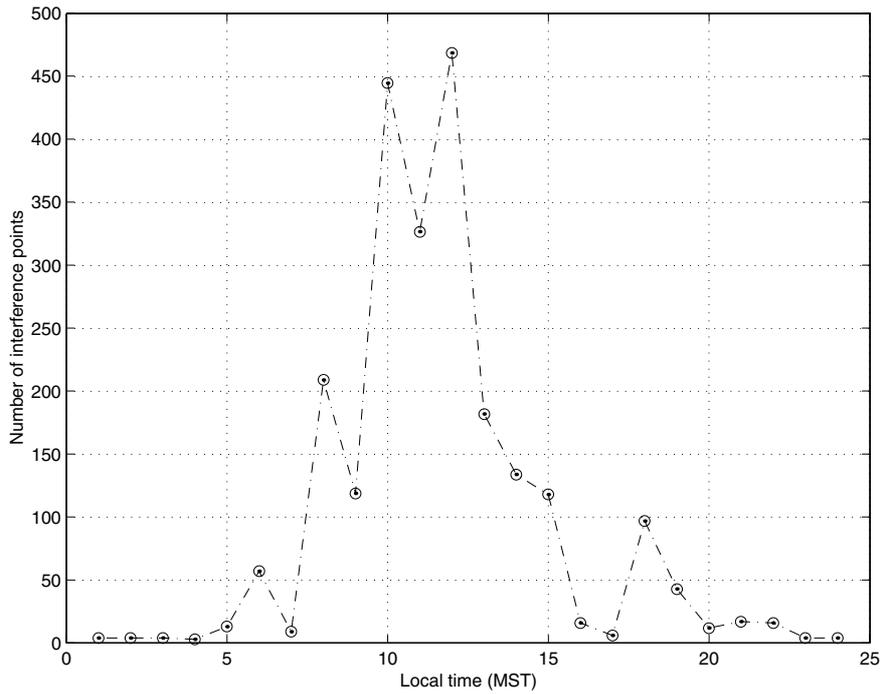


**Figure 9.** Number of interference points with MST.

occur for shorter durations ($\approx$ 80% with duration less than 6 seconds). There are generally less than 20 instances in the full 24 hours when the interference lasted 6 consecutive seconds. These statistics indicate that very often the interference excision can be carried out while post integrating the visibilities by giving a zero weighting to the interference points.

- A typical plot of number of interference points against local time (MST) in a given day is shown in Fig. 9. The interference is mostly during the day and is between MST 8:00hrs and 15:00hrs. These are the industrial working hours in Mauritius. This therefore indicates that interference is linked to the local industry.
- Figure 10 shows the number of interference points on different days during the observing period. We don't see any particular trend in the number of interferences over the year. A better indicator of any trend would require an analysis of statistics of a larger number of days.

interference points on different days during the observing schedule
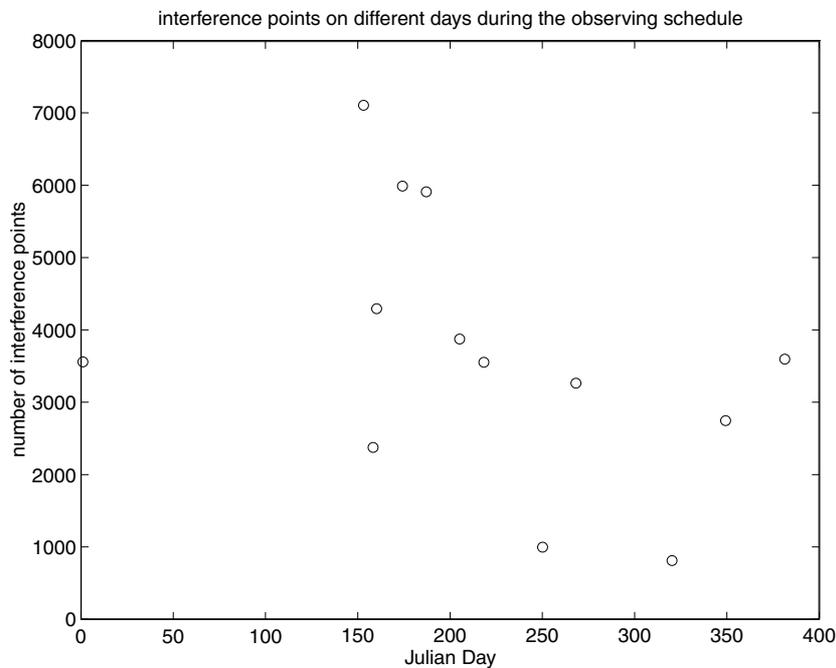


**Figure 10.** Number of interference points on different days during the observing schedule.The last three digits of the Julian Day are shown. The 0 on the *x*-axis corresponds to Julian day 2450150.

- We have found that the interference is reduced on Sundays and on other public holidays. As seen from Fig. 10, on Sunday the number of interference points could be as low as 1% of the data collected while it could be around 10% on other days.
- We note that we do not have any frequency information of the interfering signals. However we have found that the interfering signals are correlated in visibilities measured with different delay settings. The extent of the delay to which the interference is correlated gives an estimate of its bandwidth. Our measurements indicate that the interference is narrow-band ($\approx$ 10 kHz).

## 6. Interference excision

The raw data are not modified by the interference detection programs. The right ascension of the detected points are stored in a file and this information on interference is used in the subsequent calibration and imaging programs. As mentioned in the section on the observations, the visibilities are recorded with one second integration. While estimating the complex antenna gains, the file containing interference information is used to give zero weighting to the visibilities affected by interference. The measured visibilities are calibrated using the complex antenna gains estimated in the calibration process. The calibrated visibilities are box-car averaged for 4 seconds. Interference excision is incorporated at this stage by giving zero weighting to the points affected by interference. The averaged visibilities are phased appropriately to get an image on the meridian. The images of different days so obtained are precessed to a common epoch and then added. To obtain an optimum signal-to-noise ratio the images are convolved in the right ascension with a sinc function having a FWHM of 16 seconds in time. This is the FWHM in RA of the expected PSF of MRT in EW × S mode at zero degree declination. The simplicity of the method is due to the effective way the statistics of interference are used in its excision.

## 7. Conclusion

With the increasing demand for the commercial usage of the electromagnetic spectrum, it is becoming difficult to carry out radio astronomical observations, especially at low frequencies. In this environment it is most profitable to study the nature of interference at different observatory sites and develop techniques to obtain maximum interference-free observations or mitigate interference in the data recorded.

We have successfully developed a technique to detect man-made interference in the visibility data of MRT. This is a filtering technique based on the assumption that the interference is generally 'spiky' in nature and has Fourier components beyond the maximum frequency which can arise from radio sky and can therefore be identified. We take the sum of magnitudes of visibilities on all the baselines measured at a given time to improve detectability. The raw data are not modified by the interference detection programs. The right ascension of the detected points are stored in a file and this information on interference is used in the subsequent calibration and imaging programs. We have carried out statistical analysis of the interference detected. They indicate that most of the interference have strengths less than $100\sigma$ ($\approx 85\%$). The interference is largely during the day (MST 8–15 hours) and is linked to the local industry. A large fraction $\approx 80\%$ of the interference occurs for durations less than 6 seconds. There are generally less than 20 instances in the full 24 hours when the interference lasted 6 consecutive seconds. This indicates that very often the interference excision can be carried out while post integrating the visibilities by giving a zero weighting to the interference points. The level of undetected interference is of the order of the noise in the final image. This, in terms of flux density is $\approx 100$ mJy.

## References

Golap, K., Udaya Shankar, N., Sachdev, S., Dodson, R., & Sastry, Ch.V. 1998 A Low Frequency Radio Telescope at Mauritius for a Southern Sky Survey, *J. Astrophys. Astr.*, **19**, 35.

Handbook On Radio Astronomy, 1995, (Geneva: Radiocommunication Bureau).

Hogbom J.A.1974 Aperture Synthesis with a Non-Regular Distribution of Interferometer Baselines *Astrphys. J. Suppl. Ser.*, **15**, 417.

Sachdev. S., 1999, *Wide Field Imaging with the Mauritius Radio Telescope,* Ph.D. Thesis, Dept. of Physics, University Of Mauritius.